Supplemental Material: Creating and Steering Highly Directional Electron Beams in Graphene

Ming-Hao Liu (劉明豪), Cosimo Gorini, and Klaus Richter
Institut für Theoretische Physik, Universität Regensburg, D-93040 Regensburg, Germany
(Dated: December 19, 2016)

Overview

This supplemental material provides additional numerical examples of the probability current density profiles to show the influence of

(i) spatial disorder in graphene samples,

(ii) edge roughness of the parabolic gate, and

(iii) the smoothness of the *pn* junction

on the electron beam generated by the lensing apparatus described in the main text. All numerical examples are meant to be compared with (and are being based on the same parameters as) the ideal case of Fig. 1(c) in the main text, which considers a focal length $f = 200\,\mathrm{nm}$, densities $n_o = -n_i = 6\times10^{11}\,\mathrm{cm}^{-2}$ corresponding to a Fermi wave length $\lambda_F \approx 46\,\mathrm{nm}$, and a smoothness $\ell_s = 30\,\mathrm{nm}$ of the *pn* junction profile. Moreover, we comment on the expected temperature dependence in the closing.

Disorder in graphene

Throughout the main text the graphene lattice is treated as purely ballistic, *i.e.* free of disorder, in view of high mobilities for graphene achieved in state-of-the-art experiments with mean free paths ℓ_{mfp} up to scales beyond $20\,\mu\mathrm{m}$ [1]. To test the robustness of the proposed lensing apparatus against disorder, we consider a Hamiltonian with random on-site potential:

$$H = H_0 + \sum_j U_j c_j^\dagger c_j \,.$$

Here, H_0 is the clean part of the scaled tight-binding Hamiltonian [2] (including the lensing potential), and $U_j \in [-U_{\mathrm{dis}}/2, U_{\mathrm{dis}}/2]$ is a random potential at site j fluctuating in a range of U_{dis}.

As a reference panel, Fig. S1(a) shows the beam for the clean system without disorder, repeating Fig. 1(c) of the main text. In panels S1(b), (c),..., (f) we consider $U_{\mathrm{dis}} = 10\,\mathrm{meV}$, $20\,\mathrm{meV}$, ..., $50\,\mathrm{meV}$ which clearly demonstrate the robustness of the beam profile against static potential disorder. Reasonably, the generated electron beam is expected to remain focused in a range shorter than the elastic mean free path ℓ_{mfp}. Using Fermi's golden rule, in Fig. S1(b), (c), (d), (e), and (f) the mean free paths are estimated to be $\ell_{\mathrm{mfp}} \approx 106.4\,\mu\mathrm{m}$, $26.6\,\mu\mathrm{m}$, $11.8\,\mu\mathrm{m}$, $6.7\,\mu\mathrm{m}$, and $4.3\,\mu\mathrm{m}$, respectively, covering the current state-of-the-art ℓ_{mfp} of $28\,\mu\mathrm{m}$ [1]. Naturally, the lensing apparatus is expected to fail in strongly disordered graphene with $\ell_{\mathrm{mfp}} \lesssim f$. Note that the relevant transport mean free path, equal to the elastic mean free path for white-noise type disorder (*s*-wave scattering) considered here, will be even longer for long-range potential fluctuations, implying an even more robust beam profile in the latter case.

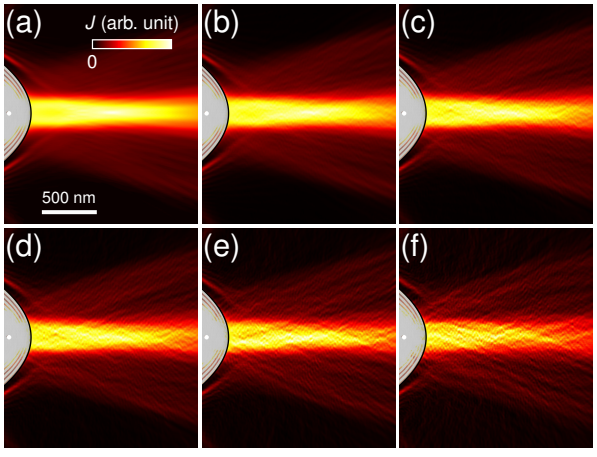

FIG. S1. Probability current density profiles of the electron beam generated by the lensing apparatus (focal length $f = 200\,\mathrm{nm}$) in the presence of (a) zero and (b)–(f) finite disorder. The disorder strengths U_{dis} in (b), ..., (f) are $10,\ldots,50\,\mathrm{meV}$. The color in (a) applies to all the J maps in this supplemental material, and so does the scale bar, except in Fig. S2(b).

Edge roughness of the parabolic gate

The parabolic *pn* junction in our lensing apparatus can be experimentally realized by a local gate etched in a parabolic shape, which is expected to be imperfect in reality. Depending on the resolution of the *e*-beam lithography and the material properties of the polymer mask used during the fabrication process, the profile of the parabolic gate may exhibit edge roughness. Based on a mathematical model estalblished for studying surface roughness [3], which was later adopted to investigate the effect of line edge roughness (LER) in graphene nanoribbons [4, 5], an example of the resulting current density J is shown in Fig. S2(a), considering rather strong LER parameters [see Fig. S2(b) for the actual edge profile considered in Fig. S2(a)].

To better quantify the effect of the edge roughness, in the following we consider a simplified model with a regular fluctuating profile perpendicular to the parabola described by $\delta\cos(2\pi s/\lambda)$, where s is the arc length of the parabola with respect to its vertex. See an exemplary sketch in Fig. S2(c).

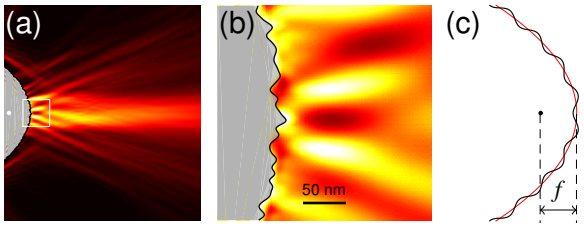

FIG. S2. (a) Imperfect beam profile considering a strong line edge roughness [3–5] (fluctuation range and correlation length $\sim 20\,\mathrm{nm}$) modulating the parabolic gate profile. The region marked by a white box is zoomed in and shown in (b). (c) Schematic of a perfect parabola (red thin line) modulated by a cosine function (black thick line) with an amplitude $\delta = f/10$ and period $\lambda = f$.

Since the edge roughness may typically fluctuate within a range of $2\delta \sim 10\,\mathrm{nm}$ [6], we consider $\delta = 3\,\mathrm{nm}$, $5\,\mathrm{nm}$, and $7\,\mathrm{nm}$ in Fig. S3, each with various roughness periodicities of $\lambda = 5\delta, 10\delta, 15\delta$ (for $\lambda = \delta$ we do not observe any observable distortion of the beam). Recall from the main text that the Fermi wave length is $\lambda_F \approx 46\,\mathrm{nm}$, which is much longer than the considered fluctuation amplitude δ. The parameter δ is therefore expected to play a minor role. On the other hand, the considered periodicities cover the case $\lambda > \lambda_F$, when the roughness is expected to show pronounced effects.

Figure S3 confirms this intuitive expectation. In panels (a)–(c) with $\delta = 3\,\mathrm{nm}$ and $\lambda = 15, 30, 45\,\mathrm{nm}$, the beam structure remains perfectly focused in all cases, even for $\lambda \approx \lambda_F$ in Fig. S3(c), where visible leakage fringes in the vicinity of the modulated parabolic junction in addition to the collimated electron beam can be observed. In Figs. S3(d)–(f) with $\delta = 5\,\mathrm{nm}$, similar patterns with nearly perfect beam structures for $\lambda = 25\,\mathrm{nm}$ (d) and $\lambda = 50\,\mathrm{nm}$ (e) are observed, while for $\lambda = 75\,\mathrm{nm} > \lambda_F$ (f) significant leakage of secondary beams can be seen. Such secondary beams follow the wavy structure of the modulated parabolic *pn* junction, and can be observed in Figs. S3(h) and (i), both with $\lambda > \lambda_F$. Despite the large fluctuation amplitude of $\delta = 7\,\mathrm{nm}$ that already exceeds the typical roughness of $2\delta \sim 10\,\mathrm{nm}$ [6], the electron beam shown in Fig. S3(g) with $\lambda = 35\,\mathrm{nm} < \lambda_F$ remains nearly perfect.

We conclude that the electron beam generated by the proposed lensing apparatus is practically insensitive to the possible edge roughness of the parabolic gate, as long as the fluctuation amplitude and correlation length of the roughness are both smaller than the Fermi wave length.

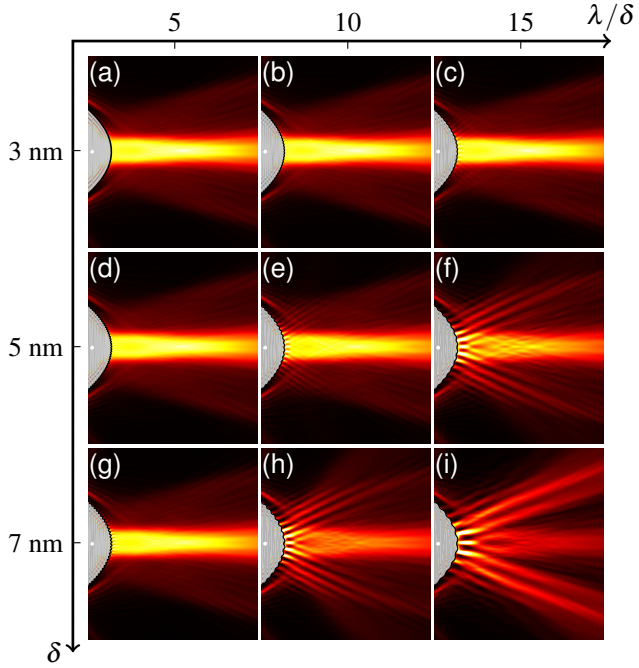

FIG. S3. Probability current density profiles of the electron beam generated by an imperfect parabolic lens based on the simplified model sketched in Fig. S2(b) with various roughness amplitudes δ (left to right panels) and periods λ (upper to lower panels).

Smoothness of the *pn* junction

In the main text, as well as in Figs. S1–S3, the carrier density function modeling the parabolic junction has been described by a smoothness of $\ell_s = 30\,\mathrm{nm}$ bridging the inner and outer densities. In experiments, the length scale of this smoothness is determined by the distance from the graphene sample to the parabolic gate. The idea of the lensing apparatus was motivated by the experimental work of [7] for point contacts in hBN-encapsulated graphene (hBN stands for hexagonal boron nitride), implying $\ell_s \sim t_{\mathrm{hBN}}$. Here t_{hBN} is the thickness of the hBN encapsulation layer separating the graphene sample and the gate electrode, and ranges typically from several to a few tens of nm. As explained in a technical remark in the main text, the chosen $\ell_s = 30\,\mathrm{nm}$ is not only a typical hBN layer thickness but also well satisfies $a \ll \ell_s$, where a is the scaled lattice spacing, required for the scalable tight-binding model (TBM) [2] to be precise enough.

Specifically, our lattice spacing scaled by a factor $s_f = 8$ is $a \approx 1\,\mathrm{nm}$, corresponding to $1/30$ of the smoothness for $\ell_s = 30\,\mathrm{nm}$ and thereby ensuring a high precision of the scalable TBM. In Fig. S4, the J profiles of the generated beam

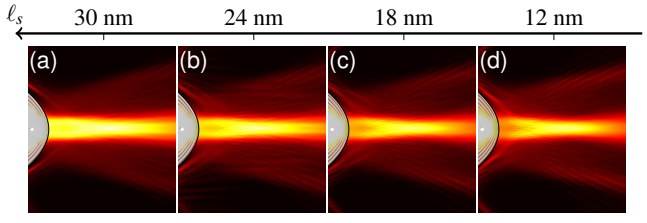

FIG. S4. Probability current density profiles of the electron beam generated by a parabolic *pn* junction with varying smoothness. Panel (a) with smoothness $\ell_s = 30\,\mathrm{nm}$, identical to Fig. S1(a), is shown for reference; panels (b)–(d) display results for sharper junctions with smaller $\ell_s = 24, 18, 12\,\mathrm{nm}$.

considering smoothness of $\ell_s = 24, 18, 12\,\mathrm{nm}$, in addition to the reference case with $\ell = 30\,\mathrm{nm}$, are shown. Clearly, the beam structure exhibits only minimal changes for reduced smoothness. The sharpest junction considered in Fig. S4(d) has $a \approx \ell_s/12 \ll \ell_s$ so that the scalable TBM should work well in all panels of Fig. S4, however we note that its slight decrease in precision from (a) to (d) may be the cause of the fine structure outside the beam vaguely visible, in particular in panel (d).

Overall, the beam structure is shown to be rather insensitive to the smoothness of the parabolic *pn* junction for typical hBN layer thicknesses sandwiching the graphene sample.

Temperature dependence

All calculations here and in the main text were done at the Fermi level and assuming zero temperature. This is a very good approximation, since most ballistic graphene transport experiments are typically performed at temperatures around 1 K. Still, we comment on possible effects on our lensing apparatus due to finite temperature.

Thermal broadening. As the energy scale of thermal broadening is around $\Delta E_{\mathrm{th}} \sim 10^{-4}\,\mathrm{eV}$ at a temperature $T = 1\,\mathrm{K}$, negligible compared to typical transport energy scales in graphene *pn* junctions, we expect the lensing apparatus to work up to a few tens of Kelvin. Specifically, the densities $n_o = -n_i = 6 \times 10^{11}\,\mathrm{cm}^{-2}$ considered in our numerical examples correspond to a Fermi energy $E_F \approx 90\,\mathrm{meV}$. Thus for the thermal broadening to be appreciable, $\Delta E_{\mathrm{th}} \sim E_F/10$, which corresponds to a temperature around 100 K.

Increased scattering rate. With increasing temperature the inelastic scattering rate due to electron-electron and electron-phonon interactions increases, and hence, vice versa, the effecive electron mean free path ℓ_{mfp} decreases once T-dependent inelastic scattering exceeds elastic potential scattering. This is the basic mechanism that e.g. suppresses the Fabry-Pérot-type interference observed in graphene *pnp* cavities of length ℓ_c when increasing the temperature from a few K (at which $\ell_{\mathrm{mfp}} > \ell_c$) to a few tens of K (at which $\ell_{\mathrm{mfp}} < \ell_c$); see, for example, [8, 9]. As shown in one of the state-of-the-art works on hBN-encapsulated graphene [10], ℓ_{mfp} indeed decreases with T exponentially but still remains several microns at temperatures as high as $T = 100\,\mathrm{K}$. Thus the proposed lensing apparatus, if carried out in such a high-quality sample, would, in principle, persist up to such temperatures. The focal length f sets the mimimum scale for ℓ_{mfp} required such that a collimated beam can be formed by the lensing apparatus.

To conclude the above discussion, the lensing mechanism proposed in the main text is not expected to be vulnerable to finite temperature. Indeed, in high-quality samples as [10] at energy scales around 0.1 eV or above, it is expected to work at temperature $T \lesssim 100\,\mathrm{K}$.

[1] L. Banszerus, M. Schmitz, S. Engels, M. Goldsche, K. Watanabe, T. Taniguchi, B. Beschoten, and C. Stampfer, Nano Letters **16**, 1387 (2016).
[2] M.-H. Liu, P. Rickhaus, P. Makk, E. Tóvári, R. Maurand, F. Tkatschenko, M. Weiss, C. Schönenberger, and K. Richter, Phys. Rev. Lett. **114**, 036601 (2015).
[3] D. K. Ferry, S. M. Goodnick, and J. Bird, *Transport in Nanostructures* (Cambridge University Press, New York, 2009).
[4] T. Fang, A. Konar, H. Xing, and D. Jena, Phys. Rev. B **78**, 205403 (2008).
[5] A. Yazdanpanah, M. Pourfath, M. Fathipour, H. Kosina, and S. Selberherr, IEEE Transactions on Electron Devices **59**, 433 (2012).
[6] C. Handschin, P. Makk, and P. Rickhaus, private communication.
[7] C. Handschin, B. Fülöp, P. Makk, S. Blanter, M. Weiss, K. Watanabe, T. Taniguchi, S. Csonka, and C. Schönenberger, Appl. Phys. Lett. **107**, 183108 (2015).
[8] A. F. Young and P. Kim, Nat. Phys. **5**, 222 (2009).
[9] A. L. Grushina, D.-K. Ki, and A. F. Morpurgo, Appl. Phys. Lett. **102**, 223102 (2013).
[10] L. Wang, I. Meric, P. Y. Huang, Q. Gao, Y. Gao, H. Tran, T. Taniguchi, K. Watanabe, L. M. Campos, D. A. Muller, J. Guo, P. Kim, J. Hone, K. L. Shepard, and C. R. Dean, Science **342**, 614 (2013).